Secular Variation candidate for the IGRF-13

Sanchez S[1], Wicht J[1], and Baerenzung J[2]

[1]Max Planck Institute for Solar System Research, Göttingen, Germany
[2]Potsdam University, Potsdam, Germany

October 1, 2019

Abstract

We present a secular variation (SV) candidate for the 13th IGRF generation for the year 2020. It is based on the evolution of an ensemble of three dimensional dynamo simulations, which assimilates the magnetic field from the COV-OBS.x1 model from 1840 to 2000 and the Kalmag main field model from 2001 to 2020. The dynamo simulation setup was chosen accordingly to its performance in hindcast tests. The tests also suggest that instantaneous SV yields better 5-year forecasts than the full dynamo dynamics. This indicates that the model overestimates the secular acceleration. We therefore propose the instantaneous SV from our assimilation for the 13th IGRF, and also provide ensemble based uncertainty estimates.

1 Method

The geomagnetic data assimilation framework employed here has been described in detail in Sanchez et al. (2019). It uses an Ensemble Kalman Filter (EnKF, Evensen, 1994) based on 3D dynamo simulations (Parody-PDAF code, see Fournier et al., 2013). An ensemble of dynamo simulations defines the background model statistics (the prior), which is combined with geomagnetic field models through a sequence of forecast and analysis cycles. The forecast is the propagation of each dynamo ensemble member from time t_{i-1} to time t_i by the numerical integration. When describing the dynamo state with vector $\mathbf{x}$ and the time propagation with the operator $\mathcal{M}$, the forecast can formally be written as:

$$\mathbf{x}^f_{i,e} = \mathcal{M}_{i,i-1}(\mathbf{x}^a_{i-1,e}) \, , \tag{1}$$

where indexes i and e correspond to time and ensemble member, respectively. Whenever observations $\mathbf{y}$ are available, the analysis step is performed, using

$$\mathbf{x}^a_{i,e} = \mathbf{x}^f_{i,e} + \mathbf{K}_i(\mathbf{y}_{i,e} - \mathbf{H}_i\mathbf{x}^f_{i,e}), \tag{2}$$

where $\mathbf{H}$ is the observation operator. The Kalman Gain matrix

$$\mathbf{K}_i = \mathbf{P}^f_i\mathbf{H}^\dagger_i(\mathbf{H}_i\mathbf{P}^f_i\mathbf{H}^\dagger_i + \mathbf{R}_i)^{-1}, \tag{3}$$

propagates information from observed to unobserved parts of the model state, where $\mathbf{P}$ and $\mathbf{R}$ are the model and observation error covariances, respectively.

In order to mitigate sampling effects due to insufficient ensemble size, we apply a spectral localization of the model covariance, of the form $\mathbf{L} \circ \mathbf{P}$, where $\mathbf{L}$ is a localization mask with either zero or unity entries. As shown in Sanchez et al. (2019), dynamo simulations suggest that the correlations between model coefficients within the same azimuthal wave number are most significant. Using a localization matrix $\mathbf{L}$ based on the same order m indeed rendered the EnKF stable when confronted with modern high accuracy observations. Here we use an additional localization based on the equatorial symmetries of the different fields of the dynamo system, as suggested in Sanchez et al. (2019). A representation of the model covariance $\mathbf{P}$ and localization matrix $\mathbf{L}$ is shown in Fig. 1. The spectral localization allows us to use a moderate ensemble size of $N_e = 256$ dynamo models.

The background dynamo simulation setup used in the assimilation closely resembles the one in Sanchez et al. (2019). It corresponds to a model with Ekman number $\mathrm{E} = 10^{-4}$, modified Rayleigh number $\mathrm{Ra}= 10^{-5}$, and magnetic Prandtl number $\mathrm{Pm}=10$. Relevant outputs are the Reynolds number $\mathrm{Re} = 43$, the magnetic Reynolds number $\mathrm{Rm} = 430$ and a marginal Earth-likeness following the criteria by Christensen et al. (2010). Time was rescaled by matching the secular variation time scale of the simulation to characteristic Earth values (Lhuillier et al., 2011). The magnetic field was rescaled so that the mean axial dipole of the initial ensemble matches the average value of the observations over the period 1840 to 2020.

Finally, the IGRF SV candidate model consists on the set of $\dot{g}^m_\ell$ coefficients truncated to spherical harmonic degree $L = 8$. The numerical dynamo model provides the instantaneous SV for each ensemble member, which then allows calculating the ensemble mean:

$$\bar{\dot{g}}^m_\ell(t) = \frac{1}{N_e}\sum_{e=1}^{N_e} \dot{g}^m_{\ell,e}(t), \tag{4}$$

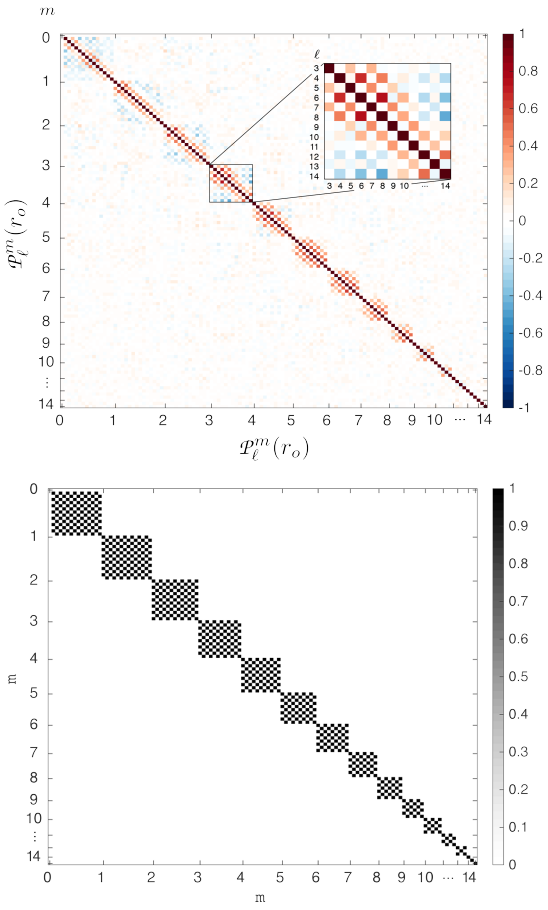

Figure 1: Top: Subset of the normalized model covariance $\mathbf{P}$, showing correlations of the poloidal magnetic field at the core surface calculated from the ensemble of dynamo simulations. Bottom: Localization matrix $\mathbf{L}$.

together with its corresponding standard deviation

$$\sigma[\dot{g}_\ell^m(t)] = \sqrt{\frac{1}{N_e - 1}\sum_{e=1}^{N_e}[\dot{g}_{\ell,e}^m(t) - \bar{\dot{g}}_\ell^m(t)]^2}, \qquad (5)$$

in units of nT/yr.

2 Observations

We assimilate the main field from two datasets: the COV-OBS.x1 model by Gillet et al. (2015) and the Kalmag model issued by the Potsdam University team led by J. Baerenzung, also participating as an IGRF-13 candidate model. COB-OBS.x1 is a model based on magnetic observatory and satellite data, spanning the years between 1840 and 2015. The Kalmag model is based solely on satellite data and spans the period from 2001 to 2020. While COV-OBS.x1's model truncation is $L = 14$, a more intricate separation of field sources of the Kalmag model allows a truncation of the main field up to $L = 20$. Both models supply uncertainties.

A comparison of the uncertainties from COV-OBS.x1 and Kalmag models reveal a growing discrepancy over the last 60 years, as shown in Fig. 2. COV-OBS.x1 uncertainties continue to decrease until 2000 and likely underestimate the true value in recent epochs (as also suggested by Barrois et al., 2018). We assume that the larger and nearly constant Kalmag uncertainties provide a more realistic value. COV-OBS.x1 uncertainties lower than Kalmag values are simply set to the Kalmag uncertainty at the year 2001 for each coefficient (blue line in Fig. 2).

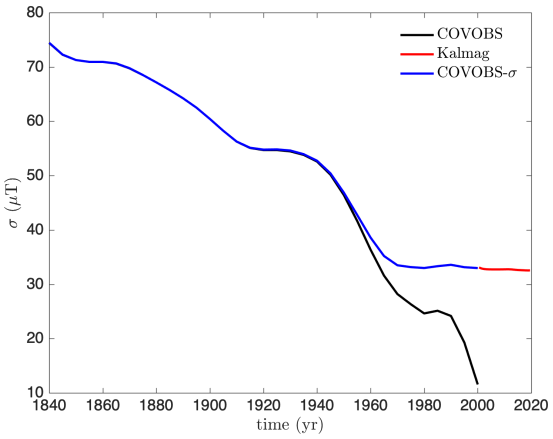

Figure 2: RMS uncertainty, evaluated at the core surface, of COV-OBS.x1 (black) and Kalmag (red) truncated to spherical harmonic degree $L = 14$. Also shown are the corrected COV-OBS.x1 uncertainties (blue).

COV-OBS.x1 is assimilated every 5 years from the year 1840 to 2000, while Kalmag is assimilated every 1 year from 2001 to 2020. The Kalmag model is assimilated up to degree $L = 18$, for beyond that the uncertainties are much too high and thought not to influence the assimilation.

3 Results

We perform a set of hindcast tests with our assimilation scheme. In these tests, the assimilation is stopped at time t_i before the end of available data, and the ensemble is free to evolve up to time t_f where data are still available, allowing for a direct comparison of forecast and observation. To judge the quality of the predictions we use CHAOS-6-x9 (Finlay et al., 2016) as a reference model. Prediction errors of the ensemble evolution are compared to predictions from a linear extrapolation with the instantaneous SV estimate. We also compare the prediction errors of previous IGRF predictions, the case where the secular variation is zero (nocast), and errors when using instantaneous CHAOS-6 SV predictions

Table 1 lists the errors from hindcasts beginning at $t_i = 2005$ and 2010 and ending at $t_f = 2010$ and 2015, respectively. The table also shows the errors from our data assimilation forecast (FC) and the extrapolation based on the instantaneous SV at t_i (I-SV) from our ensemble.

Table 1: Prediction errors evaluated at Earth's surface (RMS values) truncated to $L = 8$ and given in nT units from hindcasts performed from times t_i to f_f. The errors are calculated with respect to the CHAOS-6 model at t_f. Nocast refers to predictions in which the field remains unchanged in time, therefore with zero SV. IGRF is the prediction based on the IGRF model and its SV at t_i and C-SV is the prediction considering a linear extrapolation based on CHAOS-6 model and its instantaneous SV at t_i. I-SV is the same but based on the instantaneous SV at t_i from our assimilation scheme. FC corresponds to the prediction error from the forecast in t_f based on the evolution of the ensemble of dynamo models.

$t_f - t_i$	2010-2005	2015-2010
Nocast	313.00	343.78
IGRF	91.45	62.20
C-SV	49.80	45.29
I-SV	60.72	52.82
FC	98.76	103.61

The errors differ considerably when using the direct forecast (FC) or instantaneous (I-SV) secular variation. This indicates that the secular acceleration is too strong in the dynamo models (also pointed out by Fournier et al., 2015). Christensen et al. (2012) attribute field acceleration to flow accelerations in their dynamo models. We thus speculate that flow variations happen too fast when compared with magnetic field variations. This is consistent with the observation that the Alfven Mach number, the ratio of Alfvén to flow velocity, is too small in the dynamo simulations.

All in all, predictions based on instantaneous SV from CHAOS-6 and from our assimilation are comparable and outperform previous IGRF predictions. We decide therefore to supply our instantaneous value as a candidate SV model for the new IGRF. We present our model coefficients for the instantaneous SV in 2020 in Table 2.

4 Summary and discussion

We present a candidate SV model from 2020 resulting from the assimilation of geomagnetic field models spanning the past one and a half century using Parody-PDAF. Comparisons of hindcast prediction errors show that extrapolations based on the instantaneous SV outperform direct assimilation forecasts. The likely reason are pronounced secular acceleration in the numerical dynamo model due to too fast flow accelerations in the dynamo models. In order to mitigate this effect, previous contributions to IGRF using dynamo models have used forecasts considering a steady flow to predict the field in the next 5 years. However, using a steady flow within the EnKF can lead to a severe underestimation of the field uncertainties, since the flow variability controls the ensemble spread.

Table 2: SV coefficients and their uncertainties for 2020 in nT/yr.

ℓ	m	$\dot{g}_\ell^m$	$\dot{h}_\ell^m$	$\sigma[\dot{g}_\ell^m]$	$\sigma[\dot{h}_\ell^m]$
1	0	6.78	0.00	0.86	0.00
1	1	6.55	-24.29	1.02	1.10
2	0	-10.87	0.00	0.93	0.00
2	1	-6.67	-29.61	0.75	0.72
2	2	-2.97	-22.56	0.65	0.62
3	0	1.91	0.00	0.67	0.00
3	1	-5.79	6.52	0.54	0.59
3	2	2.62	-0.76	0.47	0.45
3	3	-12.16	0.55	0.50	0.45
4	0	-1.39	0.00	0.40	0.00
4	1	-1.62	-0.78	0.45	0.45
4	2	-5.87	6.47	0.41	0.37
4	3	5.30	3.69	0.36	0.32
4	4	-5.35	-5.22	0.33	0.35
5	0	-0.42	0.00	0.31	0.00
5	1	0.41	-0.18	0.32	0.37
5	2	-0.33	2.42	0.29	0.30
5	3	0.11	-0.51	0.29	0.28
5	4	1.52	3.25	0.22	0.22
5	5	1.71	0.40	0.24	0.28
6	0	-0.61	0.00	0.20	0.00
6	1	-0.41	-0.29	0.22	0.22
6	2	0.31	-1.66	0.23	0.22
6	3	1.45	-1.09	0.19	0.18
6	4	-1.28	0.47	0.20	0.20
6	5	-0.04	0.17	0.16	0.17
6	6	1.17	1.25	0.18	0.19
7	0	-0.19	0.00	0.12	0.00
7	1	-0.15	0.49	0.14	0.16
7	2	-0.04	0.47	0.15	0.14
7	3	0.74	-0.57	0.15	0.13
7	4	0.17	-0.19	0.14	0.13
7	5	-0.66	-1.09	0.13	0.12
7	6	-0.80	0.14	0.12	0.11
7	7	0.71	0.19	0.13	0.13
8	0	0.07	0.00	0.09	0.00
8	1	0.32	-0.43	0.10	0.10
8	2	-0.13	0.29	0.11	0.10
8	3	0.43	0.00	0.10	0.09
8	4	-0.23	0.40	0.10	0.10
8	5	0.26	-0.47	0.08	0.08
8	6	0.17	-0.30	0.08	0.09
8	7	-0.09	0.42	0.07	0.07
8	8	0.39	-0.03	0.08	0.09

References

Barrois, O., Hammer, M., Finlay, C., Martin, Y., and Gillet, N. (2018). Assimilation of ground and satellite magnetic measurements: inference of core surface magnetic and velocity field changes. *Geophysical Journal International*, 215(1):695–712.

Christensen, U., Wardinski, I., and Lesur, V. (2012). Timescales of geomagnetic secular acceleration in satellite field models and geodynamo models. *Geophysical Journal International*, 190(1):243–254.

Christensen, U. R., Aubert, J., and Hulot, G. (2010). Conditions for Earth-like geodynamo models. *Earth and Planetary Science Letters*, 296(3):487–496.

Evensen, G. (1994). Sequential data assimilation with a nonlinear quasi-geostrophic model using Monte Carlo methods to forecast error statistics. *Journal of Geophysical Research: Oceans*, 99(C5):10143–10162.

Finlay, C. C., Olsen, N., Kotsiaros, S., Gillet, N., and Tøffner-Clausen, L. (2016). Recent geomagnetic secular variation from swarm and ground observatories as estimated in the chaos-6 geomagnetic field model. *Earth, Planets and Space*, 68(1):112.

Fournier, A., Aubert, J., and Thébault, E. (2015). A candidate secular variation model for IGRF-12 based on Swarm data and inverse geodynamo modelling. *Earth, Planets and Space*, 67(1):81.

Fournier, A., Nerger, L., and Aubert, J. (2013). An ensemble Kalman filter for the time-dependent analysis of the geomagnetic field. *Geochemistry, Geophysics, Geosystems*, 14(10):4035–4043.

Gillet, N., Barrois, O., and Finlay, C. C. (2015). Stochastic forecasting of the geomagnetic field from the COV-OBS. x1 geomagnetic field model, and candidate models for IGRF-12. *Earth, Planets and Space*, 67(1):1–14.

Lhuillier, F., Fournier, A., Hulot, G., and Aubert, J. (2011). The geomagnetic secular-variation timescale in observations and numerical dynamo models. *Geophysical Research Letters*, 38(9).

Sanchez, S., Wicht, J., Bärenzung, J., and Holschneider, M. (2019). Sequential assimilation of geomagnetic observations: perspectives for the reconstruction and prediction of core dynamics. *Geophysical Journal International*, 217(2):1434–1450.

Thébault, E., Finlay, C. C., Alken, P., Beggan, C. D., Canet, E., Chulliat, A., Langlais, B., Lesur, V., Lowes, F. J., Manoj, C., et al. (2015). Evaluation of candidate geomagnetic field models for igrf-12. *Earth, Planets and Space*, 67(1):112.